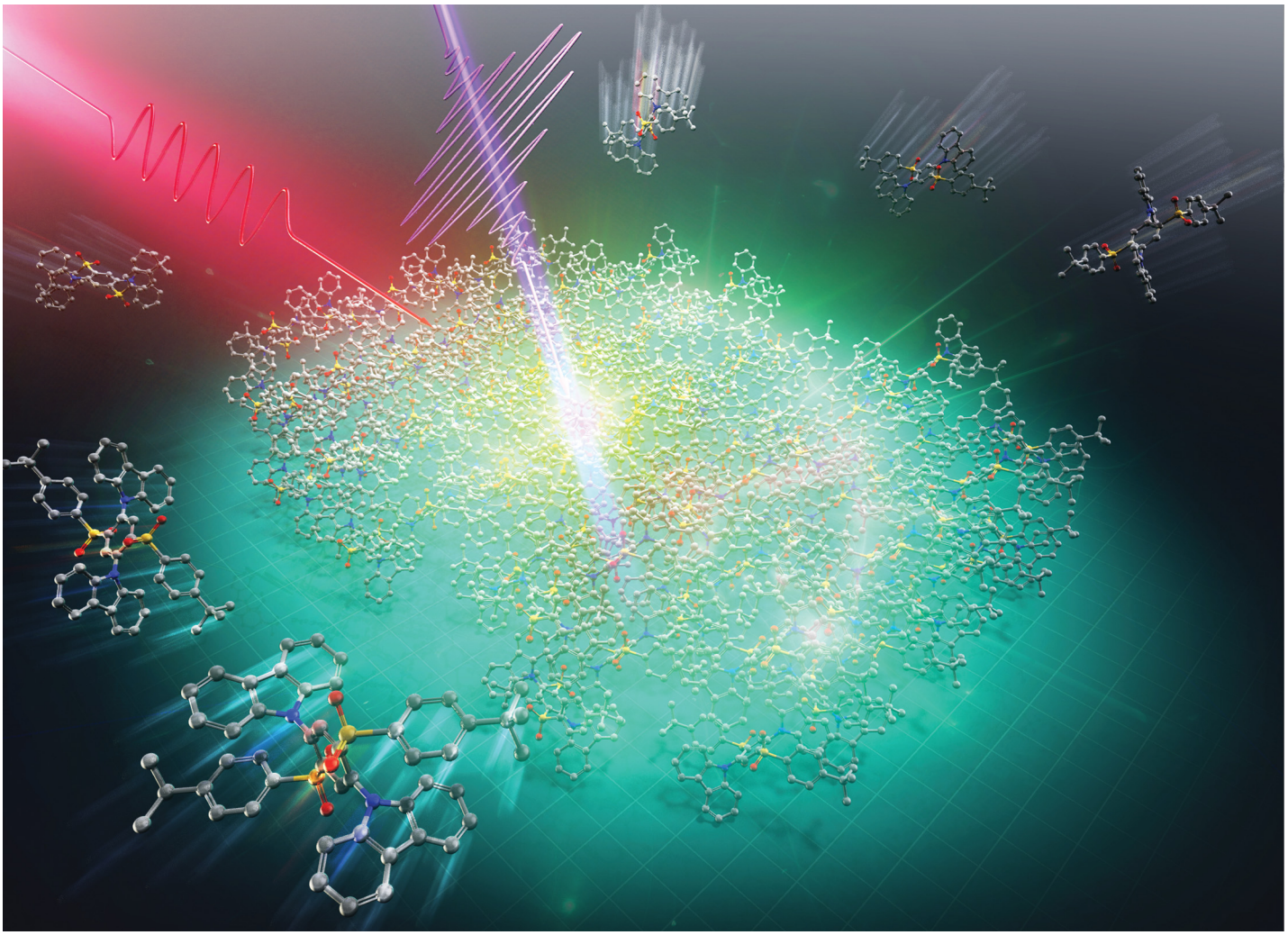

Showcasing collaborative research from Osaka Prefecture University and Kyushu University, Japan.

Aggregation-induced emission active thermally-activated delayed fluorescence materials possessing *N*-heterocycle and sulfonyl groups

A new electron-donor (carbazole)–acceptor (sulfonylbenzene) material that exhibits not only TADF but also AIE was characterized by spectroscopic analyses including time-resolved IR spectroscopy.

As featured in:

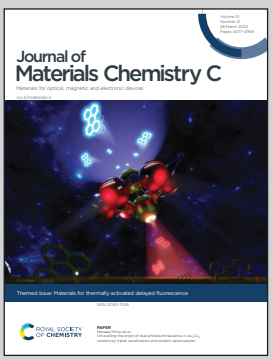

See Yasunori Matsui, Ken Onda, Hiroyoshi Naito, Hiroshi Ikeda *et al.*, *J. Mater. Chem. C*, 2022, **10**, 4607.

ROYAL SOCIETY OF CHEMISTRY

rsc.li/materials-c

Registered charity number: 207890

Journal of Materials Chemistry C

ROYAL SOCIETY OF CHEMISTRY

PAPER

View Article Online
View Journal | View Issue

Cite this: J. Mater. Chem. C, 2022, 10, 4607

Aggregation-induced emission active thermally-activated delayed fluorescence materials possessing N-heterocycle and sulfonyl groups†

Yasunori Matsui, *[ab] Yudai Yokoyama,[a] Takuya Ogaki, [ab] Kenta Ishiharaguchi,[c] Akitsugu Niwa,[c] Eisuke Ohta,[ab] Masaki Saigo,[d] Kiyoshi Miyata, [d] Ken Onda, *[d] Hiroyoshi Naito *[bc] and Hiroshi Ikeda *[ab]

Received 28th October 2021,
Accepted 10th January 2022

DOI: 10.1039/d1tc05196b

rsc.li/materials-c

Novel thermally-activated delayed fluorescence (TADF) materials 2Cz2SB and 2Mi2SB, possessing N-heterocycle and arylsulfonyl groups, were synthesized and their photophysical properties in solution and the solid state were characterized. 2Cz2SB and 2Mi2SB exhibit typical TADF characteristics and aggregation-induced emission or crystallization-induced emission behaviour. Specifically, they display a blueshift of photoluminescence wavelength and an increase in photoluminescence quantum yield (Φ_{PL}) in the aggregate and solid states, owing to suppression of thermal deactivation. The results of time-resolved IR analysis suggest that aggregate and solid state promoted suppression of geometrical changes in the excited state causes the observed increases in Φ_{PL}.

Introduction

Thermally-activated delayed fluorescence (TADF)[1,2] is a promising technology of highly-efficient organic light-emitting diodes (OLEDs).[3–5] The key process in TADF is reverse intersystem crossing (RISC), which converts a triplet excited state to the corresponding singlet-excited state (Fig. 1). RISC takes place at ambient temperatures when the gap between the singlet and triplet state energies (ΔE_{ST}) is small (<0.3 eV). Many TADF materials have been developed,[6–14] and applicated to the field of not only OLED but also imaging materials[15,16] and photosensitizers.[17–19] With the aim of improving the efficiencies of OLEDs, theoretical[20] and experimental[21,22] investigations have been carried out to uncover approaches to accelerate RISC by controlling the geometrical and electronic structures of TADF materials.

Typical TADF materials are composed of electron-donating and electron-accepting moieties that cause a reduction of ΔE_{ST}, related to spatial separation of the HOMO and LUMO. As a result, many of these materials undergo self-quenching in the solid state or in emitting layers of OLEDs, that is caused by strong intermolecular charge-transfer (CT) interactions.[23,24] Thus, the phenomenon of aggregation-induced emission (AIE),[25–28] in which aggregation leads to suppression of thermal deactivation modes, is applicable to designing efficient solid-state TADF materials. In fact, many AIE-active TADF materials have been developed to date.[29–31]

In the current investigation, which focused on the discovery of new and efficient TADF materials, we prepared 2Cz2SB and 2Mi2SB (Fig. 1) that contain a benzene core substituted by *N*-heterocycle electron-donating and *tert*-butylphenylsulfonyl electron-accepting moieties. Because the sulfonyl sulfur atom in the accepting group is sp^3-hybridized, the two π-conjugated donor and acceptor systems do not directly interact, making 2Cz2SB and 2Mi2SB potential TADF materials. In addition, para-disubstituted[32] carbazole (Cz) or 2-methylimidazole (Mi) moieties were utilized as weak electron-donors, to reduce CT interactions in the excited state.

In the effort described below, we explored the TADF and AIE characteristics of 2Cz2SB and 2Mi2SB using spectroscopic methods. The results show that these materials display excellent TADF behaviour both in solution and in the solid states. The photoluminescence quantum yields (Φ_{PL}) of 2Cz2SB and

[a] Department of Applied Chemistry, Graduate School of Engineering, Osaka Prefecture University, 1-1 Gakuen-cho, Naka-ku, Sakai, Osaka 599-8531, Japan. E-mail: ikeda@chem.osakafu-u.ac.jp
[b] The Research Institute for Molecular Electronic Devices, Osaka Prefecture University, 1-1 Gakuen-cho, Naka-ku, Sakai, Osaka 599-8531, Japan
[c] Department of Physics and Electronics, Graduate School of Engineering, Osaka Prefecture University, 1-1 Gakuen-cho, Naka-ku, Sakai, Osaka 599-8531, Japan
[d] Department of Chemistry, Graduate School of Science, Kyushu University, 774 Motooka, Nishi-ku, Fukuoka 819-0395, Japan

† Electronic supplementary information (ESI) available: General, preparation of substrates, crystal packing structure of 2Cz2SB, determination of excited state energy levels, physical properties in benzene, numerical simulations for population of excited species, fabrication of inverted OLED and device characterization, full description of TR-IR spectra, quantum chemical calculations, and NMR spectra. CCDC 2002881. For ESI and crystallographic data in CIF or other electronic format see DOI: 10.1039/d1tc05196b

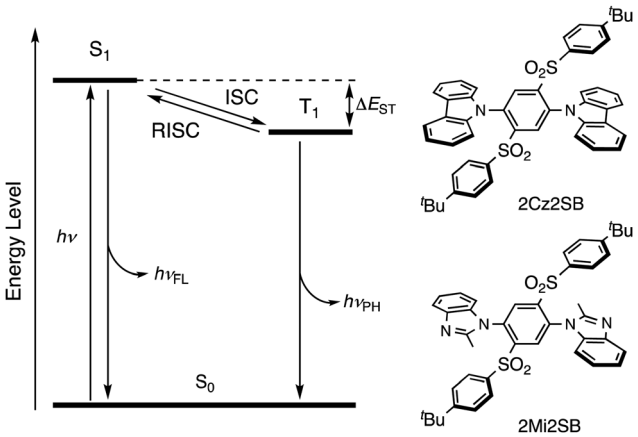

Fig. 1 Energy diagram for TADF with chemical structure of 2Cz2SB and 2Mi2SB.

2Mi2SB are increased in the crystalline or aggregate state relative to those in solution in a manner expected for operation of AIE. We also fabricated an inverted OLED using 2Cz2SB and observed that it exhibits green electroluminescence (EL).

Results and discussion

Synthesis

TADF materials 2Cz2SB and 2Mi2SB were synthesized starting with 1,2,4,5-tetrafluorobenzene by using the pathways shown in Scheme 1. Nucleophilic aromatic substitution (S_NAr) reaction of 1,2,4,5-tetrafluorobenzene with two equivalents of potassium 4-(*tert*-butyl)benzenethiolate[33] selectively produced the 1,4-substituted product **1** in 72% yield.[34] Oxidation of **1** using *m*-chloroperoxybenzoic acid (*m*CPBA) formed the corresponding sulfone **2** in excellent yield.[35] Finally, S_NAr reactions of **2** with the anions of carbazole and 2-methylimidazole generated 2Cz2SB (67%) and 2Mi2SB (32%), respectively.[36] The structures of 2Cz2SB and 2Mi2SB were characterized by using ^1H, ^{13}C NMR and IR spectroscopy, and mass spectrometric analyses. Also, the structure of 2Cz2SB was confirmed by using X-ray crystallographic analysis (Fig. 2). The manner of packing structure of 2Cz2SB has no remarkable intermolecular interactions, owing to the bulky arylsulfonyl group (Fig. S1, ESI†).

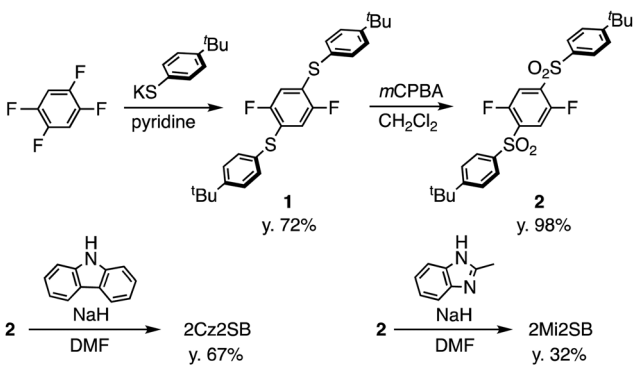

Scheme 1 Routes for synthesis of 2Cz2SB and 2Mi2SB.

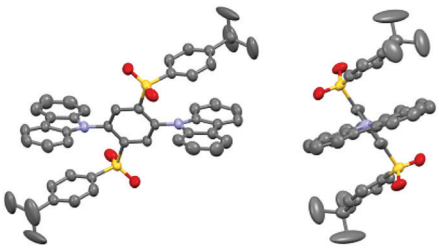

Fig. 2 ORTEP drawing of 2Cz2SB (thermal ellipsoids are shown in 50% probability).

Theoretical calculations

Density functional theory (DFT, B3LYP/6-31G(d,p)) calculations showed that the respective Cz and Mi moieties in the optimized geometries of 2Cz2SB and 2Mi2SB are highly twisted with respect to the central benzene ring. The authenticity of the calculated structure of 2Cz2SB was confirmed by using X-ray crystallographic analysis (Fig. 2). The calculations also show that the HOMO and LUMO of 2Cz2SB are localized on the electron-donating Cz and -accepting disulfonylbenzene (2SB) moieties, respectively (Fig. 3). The HOMO and LUMO of 2Mi2SB are also localized on the respective Mi and 2SB moieties. 2Mi2SB has a relatively low HOMO energy level (−6.08 eV) because of the weak electron-donating ability of the Mi moieties. The localized electronic structures of these materials lead small ΔE_{ST} values of 0.07 eV for 2Cz2SB and 0.03 eV for 2Mi2SB, determined by using time-dependent (TD)-DFT calculations. These values were in good agreement with the experimental values of ΔE_{ST} for 2Cz2SB (0.02 eV) and 2Mi2SB (0.07 eV) determined in 2-methyltetrahydrofuran matrix at 77 K (Fig. S2, ESI†). Based on the calculated wavelength of the electronic transition (λ_{ET} = 385 nm, 3.22 eV), 2Mi2SB is expected to display blue TADF.[37]

Spectroscopic measurements

UV-Vis absorption and photoluminescence (PL) spectra of solutions of 2Cz2SB and 2Mi2SB in CH_2Cl_2 were recorded (Fig. 4a). The absorption spectrum of 2Cz2SB contains a weak and broad band at λ_{AB} = 359 nm and structured bands at

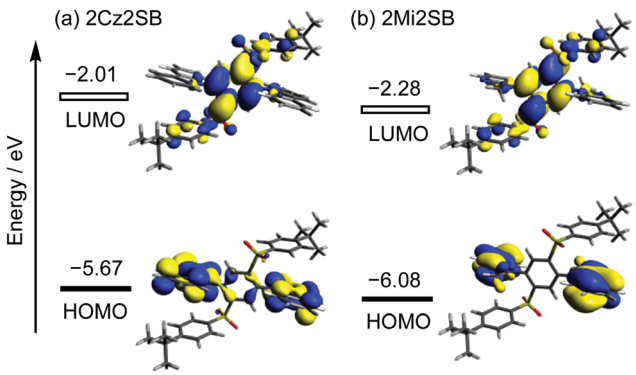

Fig. 3 Frontier molecular orbitals of (a) 2Cz2SB and (b) 2Mi2SB (B3LYP/6-31G(d,p)).

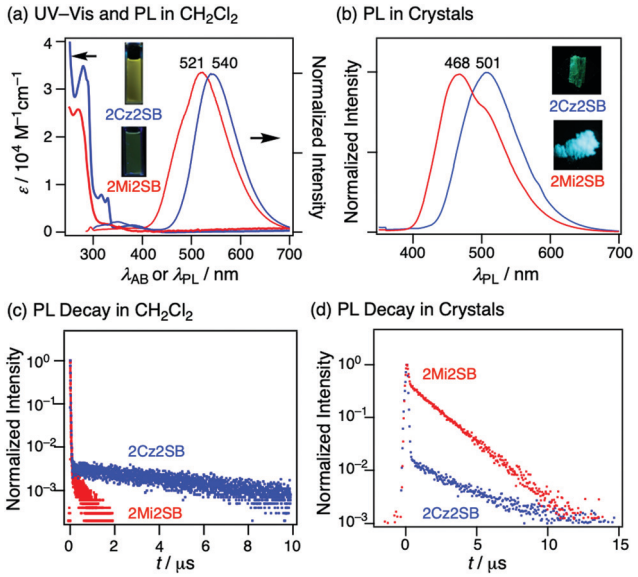

Fig. 4 (a) UV-Vis absorption and PL spectra of 2Cz2SB (blue) and 2Mi2SB (red) in CH_2Cl_2 (2×10^{-5} M, λ_{EX} = 290 nm). (b) PL spectra of crystals of 2Cz2SB and 2Mi2SB. PL decay profiles of (c) degassed CH_2Cl_2 solutions (λ_{EX} = 295 nm) and (d) crystals (λ_{EX} = 365 nm).

327 nm, assignable to intramolecular CT and π–π* transitions, respectively. The CT absorption band of 2Mi2SB at 330 nm is weak, reflecting the weak electron-donating ability of the Mi moiety. Excitation at 290 nm of these solutions led to PL at λ_{PL} = 540 and 521 nm for 2Cz2SB and 2Mi2SB, respectively. These PL maxima are greatly different from the calculated electronic transitions (429 nm for 2Cz2SB and 385 nm for 2Mi2SB), probably because of the occurrence of geometrical changes in the excited states. Analysis of the PL decay profiles of 2Cz2SB and 2Mi2SB in degassed CH_2Cl_2 (Fig. 4c), showed that the former contains prompt and delayed PL components with respective lifetimes (τ_{PL}) of 12 and 7700 ns (Table 1). Note that the delayed component was largely quenched by molecular oxygen under air. 2Mi2SB behaves similarly in that its decay profile is associated with two τ_{PL} components of 8.2 and 580 ns. The Φ_{PL} value of 2Cz2SB was determined to be 0.07 under an air atmosphere, and is increased to 0.10 under degassed conditions. Although the Φ_{PL} of 2Mi2SB is small under aerated (0.02) and degassed conditions (0.04), it is larger under Ar. The above observations indicate that 2Cz2SB and 2Mi2SB are typical TADF materials. The rate constants for ISC (k_{ISC}) and RISC (k_{RISC}) for 2Cz2SB were estimated to be the order of 10^7 and 10^4 s^{-1}, respectively, which are typical for TADF materials possessing sulfonyl groups.[14,38,39] On the other hand, k_{ISC} and k_{RISC} for 2Mi2SB were the order of 10^8 and 10^6 s^{-1}, respectively, which are much larger than those of 2Cz2SB. Although unfortunately Φ_{PL} of 2Mi2SB is not so high probably due to nonradiative deactivation, the Mi moiety can be positioned as one of the better donor parts for TADF materials.

Table 1 Photophysical properties of 2Cz2SB and 2Mi2SB in CH_2Cl_2

Material	λ_{AB} (nm)	λ_{PL} (nm)	$\tau_{PL,soln}$ (ns)	$\Phi_{PL,air}$	$\Phi_{PL,Ar}$	k_{ISC} (10^7 s^{-1})	k_{RISC} (10^4 s^{-1})
2Cz2SB	379, 329	540	12, 7700	0.07	0.10	7.7	4.3
2Mi2SB	329, 269	521	8.2, 580	0.02	0.04	11.1	175

A crystal of 2Cz2SB displays a PL band at 501 nm (Fig. 4b), which is greatly (*ca.* 40 nm) blueshifted as compared to that in CH_2Cl_2 solution. The PL decay profile of a crystal of 2Cz2SB contains prompt and delayed components with τ_{PL} of 16 and 3300 ns (Fig. 4d and Table 2). These τ_{PL} values do not change remarkably on proceeding from aerated to degassed conditions, likely because the O_2-blocking effect of crystals.[40–43] Crystals of 2Cz2SB have Φ_{PL} = 0.32, which is larger than the value in degassed CH_2Cl_2. These results show that geometrical changes that occur in the excited state in solution are largely suppressed in the crystalline state. The elongation of the prompt component in τ_{PL} (12 to 16 ns) supports this understanding. Crystals of 2Mi2SB similarly show a blueshift of 53 nm and relatively large Φ_{PL} of 0.28, possessing τ_{PL} of 38 and 1900 ns. The remarkable elongation of the prompt component in τ_{PL} (8.2 to 38 ns) are also observed for 2Mi2SB. Therefore, 2Cz2SB and 2Mi2SB have AIE or crystallization-induced emission (CIE) properties.[44]

AIE behaviour

To gain further insight into AIE characteristics, PL spectroscopic measurements were carried out of 2Cz2SB in THF/H_2O mixtures (Fig. 5). In this experiment, Φ_{PL} were determined by using an absolute method with an integrating sphere to eliminate the influence of light diffraction and optical path length changes. As compared to that in pure THF, the PL wavelength of 2Cz2SB in solutions of 0–50 vol% of H_2O content is redshifted up to 552 nm and Φ_{PL} decreases (Fig. 5b). This behaviour is associated with the increase of solvent polarity brought about by addition of H_2O, which enhances intramolecular CT interactions. On the other hand, addition of further amounts of H_2O (>75 vol%) causes an increase of Φ_{PL} to 0.196 and blueshift of λ_{PL} down to 521 nm. These changes are typical of the AIE phenomenon promoted by formation of aggregates. The PL properties of 2Cz2SB in 90 vol% of H_2O content are similar to those in the crystalline state. Therefore, the AIE characteristics of 2Cz2SB appear to be a consequence of formation of small crystal-like aggregates caused by addition of H_2O to the THF solution.

Time-resolved IR

Time-resolved IR (TR-IR) spectroscopy, a powerful tool to obtain information about geometries of excited species,[22,45–47] was carried out on 2Cz2SB in a benzene solution and KBr pellet.

Table 2 PL Properties of 2Cz2SB and 2Mi2SB in the crystalline state

Material	λ_{PL} (nm)	τ_{PL} (ns)	Φ_{PL}
2Cz2SB	501	16, 3300	0.32
2Mi2SB	468	38, 1900	0.28

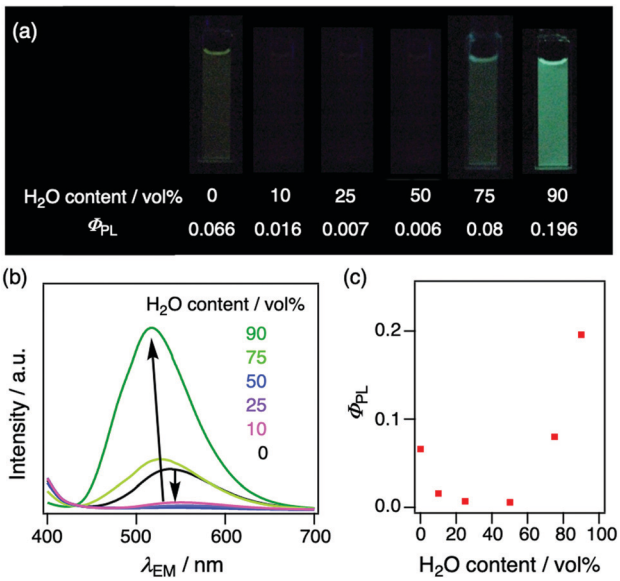

Fig. 5 (a) Photographs taken under blacklight (λ_{EX} = 365 nm), (b) PL spectra, and (c) plots of absolute Φ_{PL} against H_2O content (vol%) in THF solution of 2Cz2SB (2×10^{-5} M).

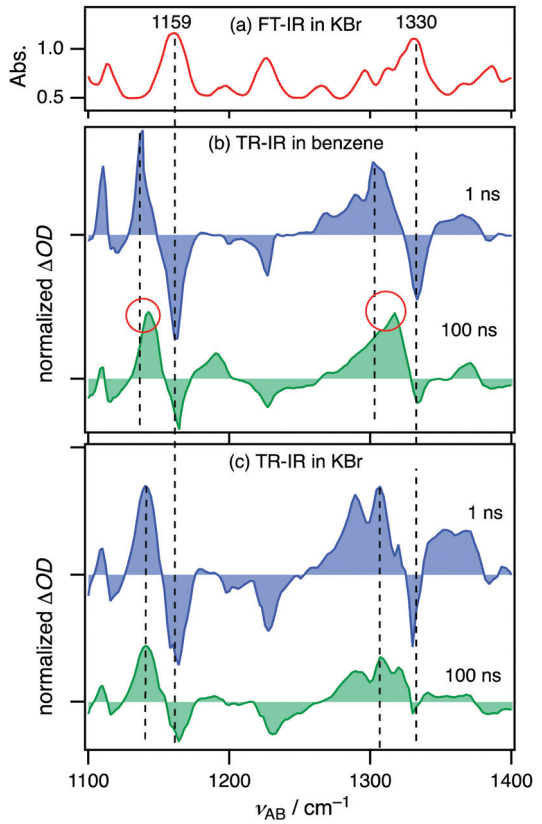

Fig. 6 (a) FT-IR spectrum of 2Cz2SB in KBr. TR-IR spectra of 2Cz2SB in (b) N_2-saturated benzene and (c) KBr. TR-IR spectra at 1 and 100 ns after photoexcitation are displayed as blue and green, respectively. Red circles indicate shift of frequencies.

An FT-IR spectrum of 2Cz2SB in KBr contains multiple bands in the 1100–1400 cm^{-1} region (Fig. 6a). By reference to known compounds[48] and quantum chemical calculations (Fig. S11, ESI†), peaks at 1159 and 1330 cm^{-1} are assignable to symmetric and asymmetric stretching of sulfonyl groups in 2Cz2SB, respectively, which were the focus of our measurements. Strong bleaching of the bands at 1159 and 1330 cm^{-1} was observed at 1 ns after 355-nm photoexcitation of 2Cz2SB in a benzene solution (Fig. 6b, blue). IR absorption bands simultaneously appear at 1138 and 1301 cm^{-1}. According to population analysis estimated by using the PL decay profile (Fig. S8, ESI†), the major excited species existing 1 ns after photoexcitation is ^{1}2Cz2SB* (^{1}2Cz2SB*/^{3}2Cz2SB* = 96/4). Thus, the 1138 and 1301 cm^{-1} peaks are assigned to symmetric and asymmetric stretching of sulfonyl groups in ^{1}2Cz2SB*, respectively. The IR absorption maxima shift to 1140 and 1316 cm^{-1} at 100 ns after photoexcitation (Fig. 6b, green). The major excited species at 100 ns after photoexcitation is ^{3}2Cz2SB* (^{1}2Cz2SB*/^{3}2Cz2SB* = 2/98) and, thus, these bands assigned to symmetric and asymmetric stretching of the sulfonyl group in ^{3}2Cz2SB*, respectively. The results show that although the SO bonds in ^{1}2Cz2SB* are considerably weakened by intramolecular CT, the strengths of those in ^{3}2Cz2SB* can be recovered by geometrical relaxation.

In contrast, TR-IR spectra of 2Cz2SB in KBr pellets did not show remarkable peak shifts between 1 and 100 ns after photoexcitation (Fig. 6c), indicating that geometrical changes between ^{1}2Cz2SB* and ^{3}2Cz2SB* in this medium are significantly suppressed. Since a suppression of geometrical change between the excited singlet and triplet states generally accelerates TADF process in carbazolyl benzonitriles,[22] this result is in good agreement with the increase of Φ_{PL} in the solid state relative to those in the solution. On the other hand, the shifts between the bleaching and the corresponding peak at 1 ns originate from the geometrical change between the ground state 2Cz2SB and the singlet excited state ^{1}2Cz2SB*. In general, the smaller geometrical change, the smaller Stokes shift. Therefore, the apparent fact that these shifts observed in KBr pellets (Fig. 6c) is smaller than those in the solution (Fig. 6b) is consistent with the blueshift of PL wavelengths of the KBr pellet.

Fabrication of inverted OLED

Because 2Cz2SB displays good TADF characteristics in the solid state, we used it to fabricate an OLED utilizing a solution process. For this purpose, we employed an inverted OLED structure, which can be simply fabricated and is air-stable.[49–53] Specifically, an ethanol solution of polyethyleneimine (PEI) was spincoated on an aluminum-zinc oxide-coated substrate to serve as an electron-injection layer. An emitting layer composed of 2Cz2SB:poly(methyl methacrylate) (PMMA) = 70/30 (wt/wt) was then spincoated on the PEI layer. After drying (60 °C, 30 min), MoO_3 and Al were vacuum-deposited as a hole-injection layer and anode, respectively. Green EL at 523 nm was observed when the external voltage of >4 V was applied to the 2Cz2SB inverted OLED (Fig. 7). The EL spectrum was nearly identical to PL spectrum (Fig. 4b) of crystals of 2Cz2SB.

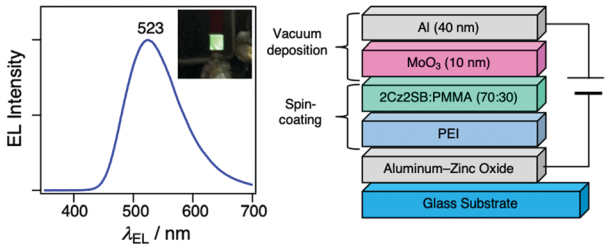

Fig. 7 An EL spectrum and device structure of the solution-processed OLED containing 2Cz2SB. (Inset: Photograph of OLED upon application of external voltage of 5 V).

The maximum current efficiency was 0.64 cd A^{-1} and can be improved by using a bipolar host matrix (electrically inactive host matrix, PMMA, was used here to form the emissive layer by means of a spin coating process).

Conclusions

In the above effort, we synthesized the novel TADF materials 2Cz2SB and 2Mi2SB bearing N-heterocycle and arylsulfonyl groups. These materials have excellent TADF characteristics both in the solution and solid states. Relative to those in solutions, the Φ_{PL} values of 2Cz2SB and 2Mi2SB are increased in the crystalline or aggregated states, which is typical AIE or CIE behaviour. We also fabricated an inverted OLED using 2Cz2SB and observed that it displays green EL. TR-IR analysis of SO-stretching vibrations revealed that the magnitude of geometrical changes in the solid state of 2Cz2SB is suppressed, demonstrating that this substance displays AIE behaviour. The above findings indicate that the arylsulfonyl group containing sp^3-hybridyzed sulfonyl sulfur atom is effective to suppress intermolecular interactions. This characteristics is also useful to create materials sensitive to external stimuli and/or environmental changes, which makes it potentially applicable to the design of a ''soft crystal''.[54]

Experimental

Preparation of materials.

The details of preparation of **1** and **2** are given in the ESI.†

1,4-Bis(9*H*-carbazol-9-yl)-2,5-bis((4-*tert*-butyl)phenylsulfonyl)-benzene (2Cz2SB). To a 100 mL round-bottom flask, carbazole (0.276 g, 1.65 mmol), NaH (60 wt% in oil dispersion, 0.075 g, 1.88 mmol), and dry DMF (25 mL) were added and stirred for 30 min at room temperature. To the solution, **2** (0.380 g, 0.750 mmol) and DMF (5 mL) was added and stirred for 26 h at 100 °C. The reaction mixture was quenched by addition of water (50 mL) and extracted with CH_2Cl_2 (50 mL × 2). The combined extracts were washed with brine, dried over Na_2SO_4, and evaporated under reduced pressure. Silica-gel column chromatography (*n*-hexane/$CHCl_3$ = 2/1) followed by recrystallization from $CHCl_3$–*n*-hexane afforded 2Cz2SB as yellow needles (405 mg, 0.51 mmol, y. 67%). mp 324 °C (differential scanning calorimetry); ^{1}H NMR (400 MHz, $CDCl_3$) δ_{ppm} 1.13 (s, 18H), 6.71 (d, J = 8.1 Hz, 4H), 6.89 (AA'BB', J = 8.7 Hz, 4H), 6.96 (AA'BB', J = 8.7 Hz, 4H), 7.20–7.33 (m, 8H), 8.11 (d, J = 8.4 Hz, 4H), 8.40 (s, 2H); ^{13}C NMR (75 MHz, $CDCl_3$) δ_{ppm} 30.9 (6C), 35.0 (2C), 110.4 (4C), 120.1 (4C), 121.9 (4C), 123.8 (4C), 125.6 (4C), 126.2 (4C), 127.9 (4C), 134.2 (2C), 134.6 (2C), 137.7 (2C), 142.1 (4C), 149.1 (2C), 157.9 (2C); IR (ATR) ν/cm^{-1} 1477, 1330, 1220, 1157, 1093, 840, 748, 722, 664; anal. calcd. for $C_{50}H_{44}N_2O_4S_2$: C, 74.97; H, 5.54 N, 3.50. Found: C, 74.72; H, 5.42; N, 3.68.

1,4-Bis(2-methylbenzoimidazol-1-yl)-2,5-bis((4-*tert*-butyl)phenylsulfonyl)benzene (2Mi2SB). To a 100 mL round bottom flask, 2-methylbenzoimidazole (0.437 g, 3.3 mmol), NaH (60 wt% oil dispersion, 0.15 g, 3.8 mmol), and DMF (50 mL) were added and stirred for 30 min at room temperature under Ar atmosphere. After addition of **2** (0.761 g, 1.5 mmol), the mixture was stirred for 20 min at 100 °C. After cooling to room temperature, the mixture was quenched by addition of water (50 mL). The mixture was extracted by CH_2Cl_2 (100 mL × 2) and then dried over Na_2SO_4. The solution was concentrated to dryness under reduced pressure and the obtained solid was washed with EtOH. Recrystallization from $CHCl_3$–*n*-hexane gave 2Mi2SB as colourless powder (0.350 g, 0.48 mmol, y. 32%). mp > 300 °C; ^{1}H NMR (400 MHz, $CDCl_3$) δ_{ppm} 1.20 (s, 18H), 2.45 (s, 6H), 6.16 (d, J = 8.0 Hz, 2H), 6.85 (dd, J = 8.0 Hz, 7.6 Hz, 2H), 7.04 (AA'BB', J = 8.0 Hz, 4H), 7.07 (AA'BB', J = 8.0 Hz, 4H), 7.19 (dd, J = 7.6 Hz, 7.6 Hz, 2H), 7.72 (d, J = 7.6 Hz, 2H), 8.40 (s, 2H); ^{13}C NMR (100 MHz, $CDCl_3$) δ_{ppm} 14.6 (2C), 30.9 (6C), 35.2 (2C), 108.8 (2C), 119.2 (2C), 122.9 (2C), 123.2 (2C), 126.3 (4C), 127.8 (4C), 133.6 (2C), 134.2 (2C), 136.2 (2C), 136.7 (4C), 142.4 (2C), 147.3 (2C), 152.3 (2C), 158.8 (2C); IR (ATR) ν/cm^{-1} 1483, 1390, 1323, 1161, 1094, 833, 740, 687, 652, 626; HR-MS (ESI+) m/z = 731.2710 (calcd. for $C_{42}H_{43}N_4O_4S_2$ $(M + H)^+$, 731.2726). anal. calcd. for $C_{42}H_{42}N_4O_4S_2$: C, 69.02; H, 5.79; N, 7.67; found: C, 67.64; H, 5.51; N 7.51.

Crystallographic analysis

X-Ray crystallographic analysis of single crystals of 2Cz2SB was performed on a Rigaku R-AXIS RAPID diffractometer using multi-layer mirror monochromated Mo-Kα radiation (λ = 0.71075 Å) at 296 K. Crystal structure refinement was carried out using SHELXL[55] and Yadokari-XG 2009.[56] Crystal data for 2Cz2SB: a colourless block crystal, $C_{50}H_{44}N_2O_4S_2$, M_w = 800.99, crystal dimensions 0.80 × 0.50 × 0.80 mm, triclinic, space group $P\bar{1}$, a = 10.6264(8), b = 13.5683(12), c = 14.6053(13) Å, α = 86.590(3)°, β = 87.124(2)°, γ = 78.622(2)°, V = 2059.2(3) Å^3, Z = 2, d = 1.292 g cm^{-3}, 9151 reflections collected, 5586 independent (R_{int} = 0.0259), GOF = 1.030, R_1 = 0.0728 ($I > 2.00\ \sigma(I)$), wR_2 = 0.2052 for all reflections. The CIF file is deposited to Cambridge Crystallographic Data Centre (CCDC†) (ID = 2002881).

TR-IR spectroscopic measurements

TR-IR measurements were performed using home-built setups with pump–probe scheme. The sample solutions were continuously circulated through a home-built IR cell equipped with BaF_2 windows with an optical path length of 0.1 mm. A probe

pulse passed through the IR cell was dispersed by a 19 cm polychromator, followed by detection using a 64-channel mercury cadmium telluride IR detector array. All measurements in 0.9 mM benzene solutions were performed after 1 h N_2-prebubbling and while bubbling maintained. For the measurement of KBr pellets, the samples were prepared by mixing 2 mg of 2Cz2SB and 100 mg of ground KBr and by pressing it in a die, forming a pellet with diameter of 13.0 mm and thickness of 0.5 mm. The details were given in the ESI† and previous reports.[46,47,57]

Theoretical calculations

Theoretical calculations on 2Cz2SB and 2Mi2SB were performed by using various functionals and 6-31G(d,p) basis set on Gaussian 09.[58] The M06-2X or PBE0 functional provided relatively reproductive IR spectra of ground state of 2Cz2SB (Fig. S11, ESI†). Unfortunately, geometries of 2Cz2SB in the singlet excited and triplet excited states reproducing TR-IR spectra cannot be found, due to complicated conformational changes of arylsulfonyl groups.

Author contributions

Y. M., H. I., and H. N. designed this research project. Y. Y. and T. O. synthesized molecules. Y. M., Y. Y., T. O., M. S. and K. M. measured photophysical properties. K. I. and A. N. fabricated OLED device under the supervision of H. N. M. S. and K. M. measured TR-IR spectra under the supervision of K. O. manuscript was prepared by contribution of all authors. All authors approved the final version of the manuscript.

Conflicts of interest

There are no conflicts to declare.

Acknowledgements

This paper is dedicated to the memory of Emeritus Prof. Toshio Mukai and Emeritus Prof. Tsutomu Miyashi at Tohoku University. This study was partially supported by JSPS KAKENHI Grant Numbers JP17H06371, JP17H06375, JP18K14202, JP19H00888, JP19H02599, JP20H02716, JP20H05106, JP20K15264, JP20K21007, JP21H04564, JP21H05494, and JP24109009. KM also acknowledges support of Qdai-jump Research Program Wakaba Challenge.

Notes and references

1 H. Uoyama, K. Goushi, K. Shizu, H. Nomura and C. Adachi, *Nature*, 2012, **492**, 234–238.
2 C. Adachi, *Jpn. J. Appl. Phys.*, 2014, **53**, 60101.
3 C. W. Tang and S. A. VanSlyke, *Appl. Phys. Lett.*, 1987, **51**, 913–915.
4 Q. Peng, A. Obolda, M. Zhang and F. Li, *Angew. Chem., Int. Ed.*, 2015, **54**, 7091–7095.
5 R. Nagata, H. Nakanotani, W. J. Potscavage and C. Adachi, *Adv. Mater.*, 2018, **30**, 1801484.
6 J. Nishida, Y. Kawakami, S. Yamamoto, Y. Matsui, H. Ikeda, Y. Hirao and T. Kawase, *Eur. J. Org. Chem.*, 2019, 3735–3743.
7 H. Kaji, H. Suzuki, T. Fukushima, K. Shizu, K. Suzuki, S. Kubo, T. Komino, H. Oiwa, F. Suzuki, A. Wakamiya, Y. Murata and C. Adachi, *Nat. Commun.*, 2015, **6**, 1–8.
8 T. Sato, M. Uejima, K. Tanaka, H. Kaji and C. Adachi, *J. Mater. Chem. C*, 2015, **3**, 870–878.
9 G. H. Kim, R. Lampande, J. B. Im, J. M. Lee, J. Y. Lee and J. H. Kwon, *Mater. Horiz.*, 2017, **4**, 619–624.
10 A. Klimash, P. Pander, W. T. Klooster, S. J. Coles, P. Data, F. B. Dias and P. J. Skabara, *J. Mater. Chem. C*, 2018, **6**, 10557–10568.
11 E. Spuling, N. Sharma, I. D. W. Samuel, E. Zysman-Colman and S. Bräse, *Chem. Commun.*, 2018, **54**, 9278–9281.
12 T. Hatakeyama, K. Shiren, K. Nakajima, S. Nomura, S. Nakatsuka, K. Kinoshita, J. Ni, Y. Ono and T. Ikuta, *Adv. Mater.*, 2016, **28**, 2777–2781.
13 Y. Kondo, K. Yoshiura, S. Kitera, H. Nishi, S. Oda, H. Gotoh, Y. Sasada, M. Yanai and T. Hatakeyama, *Nat. Photonics*, 2019, **13**, 678–682.
14 Q. Zhang, J. Li, K. Shizu, S. Huang, S. Hirata, H. Miyazaki and C. Adachi, *J. Am. Chem. Soc.*, 2012, **134**, 14706–14709.
15 X. Xiong, F. Song, J. Wang, Y. Zhang, Y. Xue, L. Sun, N. Jiang, P. Gao, L. Tian and X. Peng, *J. Am. Chem. Soc.*, 2014, **136**, 9590–9597.
16 F. Ni, Z. Zhu, X. Tong, M. Xie, Q. Zhao, C. Zhong, Y. Zou and C. Yang, *Chem. Sci.*, 2018, **9**, 6150–6155.
17 J. Lu, B. Pattengale, Q. Liu, S. Yang, W. Shi, S. Li, J. Huang and J. Zhang, *J. Am. Chem. Soc.*, 2018, **140**, 13719–13725.
18 T.-Y. Shang, L.-H. Lu, Z. Cao, Y. Liu, W.-M. He and B. Yu, *Chem. Commun.*, 2019, **55**, 5408–5419.
19 E. Speckmeier, T. G. Fischer and K. Zeitler, *J. Am. Chem. Soc.*, 2018, **140**, 15353–15365.
20 H. Noda, X.-K. Chen, H. Nakanotani, T. Hosokai, M. Miyajima, N. Notsuka, Y. Kashima, J.-L. Brédas and C. Adachi, *Nat. Mater.*, 2019, **18**, 1084–1090.
21 T. Kobayashi, A. Niwa, K. Takaki, S. Haseyama, T. Nagase, K. Goushi, C. Adachi and H. Naito, *Phys. Rev. Appl.*, 2017, **7**, 34002.
22 M. Saigo, K. Miyata, S. Tanaka, H. Nakanotani, C. Adachi and K. Onda, *J. Phys. Chem. Lett.*, 2019, **10**, 2475–2480.
23 H. S. Kim, S.-R. Park and M. C. Suh, *J. Phys. Chem. C*, 2017, **121**, 13986–13997.
24 J. Lee, N. Aizawa, M. Numata, C. Adachi and T. Yasuda, *Adv. Mater.*, 2017, **29**, 1604856.
25 J. Luo, Z. Xie, J. W. Y. Lam, L. Cheng, H. Chen, C. Qiu, H. S. Kwok, X. Zhan, Y. Liu, D. Zhu and B. Z. Tang, *Chem. Commun.*, 2001, 1740–1741.
26 Y. Hong, J. W. Y. Lam and B. Z. Tang, *Chem. Soc. Rev.*, 2011, **40**, 5361–5388.
27 S. Suzuki, S. Sasaki, A. S. Sairi, R. Iwai, B. Z. Tang and G. Konishi, *Angew. Chem., Int. Ed.*, 2020, **59**, 9856–9867.
28 T. Beppu, S. Kawata, N. Aizawa, Y.-J. Pu, Y. Abe, Y. Ohba and H. Katagiri, *ChemPlusChem*, 2014, **79**, 536–545.

29 J. Yang, M. Fang and Z. Li, *Aggregate*, 2020, **1**, 6–18.
30 S. Xu, T. Liu, Y. Mu, Y.-F. Wang, Z. Chi, C.-C. Lo, S. Liu, Y. Zhang, A. Lien and J. Xu, *Angew. Chem., Int. Ed.*, 2015, **54**, 874–878.
31 J. Guo, J. Fan, L. Lin, J. Zeng, H. Liu, C.-K. Wang, Z. Zhao and B. Z. Tang, *Adv. Sci.*, 2019, **6**, 1801629.
32 T. Hosokai, H. Matsuzaki, H. Nakanotani, K. Tokumaru, T. Tsutsui, A. Furube, K. Nasu, H. Nomura, M. Yahiro and C. Adachi, *Sci. Adv.*, 2017, **3**, e1603282.
33 B. B. Jarvis and G. P. Stahly, *J. Org. Chem.*, 1980, **45**, 2604–2609.
34 P. Robson, T. A. Smith, R. Stephens and J. C. Tatlow, *J. Chem. Soc.*, 1963, 3692–3703.
35 X.-P. Zhou, Z. Xu, M. Zeller, A. D. Hunter, S. S.-Y. Chui and C.-M. Che, *Inorg. Chem.*, 2011, **50**, 7142–7149.
36 N. Jürgensen, A. Kretzschmar, S. Höfle, J. Freudenberg, U. H. F. Bunz and G. Hernandez-Sosa, *Chem. Mater.*, 2017, **29**, 9154–9161.
37 A. Monkman, *ACS Appl. Mater. Interfaces*, 2021, DOI: 10.1021/acsami.1c09189.
38 R. Guo, P. Leng, Q. Zhang, Y. Wang, X. Lv, S. Sun, S. Ye, Y. Duan and L. Wang, *Dyes Pigm.*, 2021, **184**, 108781.
39 D. Zhou, C. H. Ryoo, D. Liu, S. Wang, G. Qian, Y. Zheng, S. Y. Park, W. Zhu and Y. Wang, *Adv. Opt. Mater.*, 2020, **8**, 1901021.
40 J. Yang, X. Zhen, B. Wang, X. Gao, Z. Ren, J. Wang, Y. Xie, J. Li, Q. Peng, K. Pu and Z. Li, *Nat. Commun.*, 2018, **9**, 840.
41 M. Shimizu, R. Shigitani, M. Nakatani, K. Kuwabara, Y. Miyake, K. Tajima, H. Sakai and T. Hasobe, *J. Phys. Chem. C*, 2016, **120**, 11631–11639.
42 A. Sakai, E. Ohta, Y. Matsui, S. Tsuzuki and H. Ikeda, *ChemPhysChem*, 2016, **17**, 4033–4036.
43 M. Shimizu, A. Kimura and H. Sakaguchi, *Eur. J. Org. Chem.*, 2016, 467–473.
44 Y. Dong, J. W. Y. Lam, A. Qin, Z. Li, J. Sun, H. H.-Y. Sung, I. D. Williams and B. Z. Tang, *Chem. Commun.*, 2007, 40–42.
45 Y. Shimoda, K. Miyata, M. Saigo, Y. Tsuchiya, C. Adachi and K. Onda, *J. Chem. Phys.*, 2020, **153**, 204702.
46 K. Koike, D. C. Grills, Y. Tamaki, E. Fujita, K. Okubo, Y. Yamazaki, M. Saigo, T. Mukuta, K. Onda and O. Ishitani, *Chem. Sci.*, 2018, **9**, 2961–2974.
47 T. Mukuta, S. Tanaka, A. Inagaki, S. Koshihara and K. Onda, *ChemistrySelect*, 2016, **1**, 2802–2807.
48 R. M. Silverstein, F. X. Webster and D. J. Kiemle, *Spectrometric Identification of Organic Compounds*, John Wiley, 7th edn, 2005.
49 K. Morii, M. Ishida, T. Takashima, T. Shimoda, Q. Wang, M. K. Nazeeruddin and M. Grätzel, *Appl. Phys. Lett.*, 2006, **89**, 183510.
50 H. Fukagawa, K. Morii, M. Hasegawa, Y. Arimoto, T. Kamada, T. Shimizu and T. Yamamoto, *Appl. Phys. Express*, 2014, **7**, 82104.
51 M. Takada, T. Nagase, T. Kobayashi and H. Naito, *Org. Electron.*, 2017, **50**, 290–295.
52 M. Takada, T. Kobayashi, T. Nagase and H. Naito, *Jpn. J. Appl. Phys.*, 2016, **55**, 03DC06.
53 M. Takada and H. Naito, in *New Polymeric Materials Based on Element-Blocks*, ed. Y. Chujo, Springer Singapore, Singapore, 2019, pp. 413–422.
54 M. Kato, H. Ito, M. Hasegawa and K. Ishii, *Chem. – Eur. J.*, 2019, **25**, 5105–5112.
55 G. M. Sheldrick, *Acta Crystallogr., Sect. C: Struct. Chem.*, 2015, **71**, 3–8.
56 C. Kabuto, S. Akine, T. Nemoto and E. Kwon, *J. Cryst. Soc. Jpn.*, 2009, **51**, 218–224.
57 T. Mukuta, N. Fukazawa, K. Murata, A. Inagaki, M. Akita, S. Tanaka, S. Koshihara and K. Onda, *Inorg. Chem.*, 2014, **53**, 2481–2490.
58 M. J. Frisch, G. W. Trucks, H. B. Schlegel, G. E. Scuseria, M. A. Robb, J. R. Cheeseman, G. Scalmani, V. Barone, B. Mennucci, G. A. Petersson, H. Nakatsuji, M. Caricato, X. Li, H. P. Hratchian, A. F. Izmaylov, J. Bloino, G. Zheng, J. L. Sonnenberg, M. Hada, M. Ehara, K. Toyota, R. Fukuda, J. Hasegawa, M. Ishida, T. Nakajima, Y. Honda, O. Kitao, H. Nakai, T. Vreven, J. A. Montgomery Jr., J. E. Peralta, F. Ogliaro, M. Bearpark, J. J. Heyd, E. Brothers, K. N. Kudin, V. N. Staroverov, R. Kobayashi, J. Normand, K. Raghavachari, A. Rendell, J. C. Burant, S. S. Iyengar, J. Tomasi, M. Cossi, N. Rega, J. M. Millam, M. Klene, J. E. Knox, J. B. Cross, V. Bakken, C. Adamo, J. Jaramillo, R. Gomperts, R. E. Stratmann, O. Yazyev, A. J. Austin, R. Cammi, C. Pomelli, J. W. Ochterski, R. L. Martin, K. Morokuma, V. G. Zakrzewski, G. A. Voth, P. Salvador, J. J. Dannenberg, S. Dapprich, A. D. Daniels, Ö. Farkas, J. B. Foresman, J. V. Ortiz, J. Cioslowski and D. J. Fox, *Gaussian 09*, 2009.